Shortcuts of freely relaxing systems using equilibrium physical observables

Isidoro González-Adalid Pemartín,[1] Emanuel Mompó,[2, 3] Antonio
Lasanta,[4, 5, *] Víctor Martín-Mayor,[1, 6] and Jesús Salas[7, 8]

[1]*Departamento de Física Teórica, Universidad Complutense, 28040 Madrid, Spain*
[2]*Departamento de Matemática Aplicada, Grupo de Dinámica No Lineal,*
Universidad Pontificia Comillas, Alberto Aguilera 25, 28015 Madrid, Spain
[3]*Instituto de Investigación Tecnológica (IIT), Universidad Pontificia Comillas, 28015 Madrid, Spain*
[4]*Departamento de Álgebra, Facultad de Educación, Economía y Tecnología de Ceuta,*
Universidad de Granada, Cortadura del Valle, s/n, 51001 Ceuta, Spain
[5]*Nanoparticles Trapping Laboratory, Universidad de Granada, Granada, Spain*
[6]*Instituto de Biocomputación y Física de Sistemas Complejos (BIFI), 50018 Zaragoza, Spain*
[7]*Departamento de Matemáticas, Universidad Carlos III de Madrid, 28911 Leganés, Spain*
[8]*Grupo de Teorías de Campos y Física Estadística,*
Instituto Gregorio Millán, Universidad Carlos III de Madrid,
Unidad Asociada al Instituto de Estructura de la Materia, CSIC, Spain
(Dated: August 9, 2023; Revised: January 9, 2024)

Many systems, when initially placed far from equilibrium, exhibit surprising behavior in their attempt to equilibrate. Striking examples are the Mpemba effect and the cooling-heating asymmetry. These anomalous behaviors can be exploited to shorten the time needed to cool down (or heat up) a system. Though, a strategy to design these effects in mesoscopic systems is missing. We bring forward a description that allows us to formulate such strategies, and, along the way, makes natural these paradoxical behaviors. In particular, we study the evolution of macroscopic physical observables of systems freely relaxing under the influence of one or two instantaneous thermal quenches. The two crucial ingredients in our approach are timescale separation and a nonmonotonic temperature evolution of an important state function. We argue that both are generic features near a first-order transition. Our theory is exemplified with the one-dimensional Ising model in a magnetic field using analytic results and numerical experiments.

Introduction. Controlling and predicting relaxation processes far from equilibrium is still an open task. In spite of historical advances mostly achieved along the 20th century [1–6], with the exception of some cases in molecular gases [7, 8], we lack a general theory beyond the linear response theory and fluctuation theorems allowing us to manage transient regimes and, in particular, optimize relaxation times of a freely evolving system between two desired states [9]. Recent progress unraveling anomalous relaxation processes in out-of-equilibrium systems points in that direction.

An outstanding example is the Mpemba effect (ME) [10–12]. Put instantly two systems—identical but for their different initial temperatures—in contact with a thermal bath at a colder-than-both temperature. The ME happens when the initially hotter system cools faster than the system that was initially closer to equilibrium.

In Markovian systems, the ME can be well understood using a spectral decomposition and diminishing or canceling slow-decaying modes for the sake of enhancing the fast ones. This has been done both in classical [13–20] and open quantum systems [21–23]. Meanwhile, in systems where spectral methods are not applicable, other strategies can be used for controlling fast and slow evolution using macroscopic observables. Namely, energy nonequipartition in water [24], a particular condition in kurtosis in granular gases [25–27], and correlation length in spin glasses [28]. Furthermore, other strategies using several quenches have been shown to be useful in attaining a speedup in relaxation times: preheating protocols [29], taking advantage of magnetic domains growth when a large number of degrees of freedom near phase transitions are present in the system and timescale separation is not possible [30], or different control techniques [31, 32].

We shall not overlook that achieving a speedup is not a trivial task. As it has been experimentally shown, the Kovacs effect prevents fast relaxation when using two quenches in a naive way, either for heating or cooling [33–36]. What is even more surprising is that, recently, another anomaly which was verified both theoretically and experimentally has been found: far from equilibrium, there can appear an asymmetry between equidistant and symmetric heating and cooling processes [37, 38]. Even more fundamental is that, using reciprocal relaxation processes between two fixed temperatures, the asymmetry is also found [38]. This has been successfully explained using the so-called "thermal kinematics" [38] based on information geometry [39, 40].

Here, we aim to control the out-of-equilibrium evolution of a system *solely* relying on its in-equilibrium physical observables and on the spectral decomposition of the dynamic-generating matrix. Our focus is on observable dynamics: clever computational speedups lacking an experimental counterpart (think, e.g., of Ref. [41]) are excluded. The physical interpretation is straightforward.

By identifying the slowest-decaying physical observables, we are able to project the system under study onto the faster ones in order to speed up the total relaxation of the system. Near first order phase transitions, the desired fast relaxation can be achieved choosing the appropriate initial condition, or, previous to the final relaxation, by briefly heating or cooling the system. To showcase this, we use the antiferromagnetic (AF) 1D Ising model with a magnetic field.

Theoretical framework. We shall model the microscopic dynamics in contact with a thermal bath at temperature T_b through a Markov dynamics with continuous time [42], obtained as the continuous limit of some discrete-time Markov chain (in our case, heat-bath dynamics [43]).

There are two complementary viewpoints on Markov dynamics. Either one considers the time evolution of the probability distribution function (the so-called strong form of the associated stochastic differential equation), or one focuses on the time evolution of observable magnitudes (the weak form) [44]. While the strong form has been emphasized in recent work [32], we shall privilege the very insightful weak-form approach. We briefly recall now the main ingredients of both approaches (see [42, 45] for details).

Let Ω be the set of all possible states of a system [46]. The strong form of the dynamics focus on the master equation for $P_{\boldsymbol{y}}^{(t)}$, the probability of finding the system in the microscopic state $\boldsymbol{y}$ at time t:

$$\frac{\mathrm{d}P_{\boldsymbol{y}}^{(t)}}{\mathrm{d}t} = \frac{1}{\tau_0} \sum_{\boldsymbol{x} \in \Omega} P_{\boldsymbol{x}}^{(t)} R_{\boldsymbol{x},\boldsymbol{y}}, \qquad (1)$$

where $R_{\boldsymbol{x},\boldsymbol{y}}/\tau_0$ is the probability per unit time for the system to jump from state $\boldsymbol{x}$ to state $\boldsymbol{y}$ when subject to a thermal bath with temperature T_b (τ_0 is a fixed time unit). Setting the diagonal term as $R_{\boldsymbol{x},\boldsymbol{x}} = -\sum_{\boldsymbol{y} \in \Omega \setminus \{\boldsymbol{x}\}} R_{\boldsymbol{x},\boldsymbol{y}}$ ensures the conservation of the total probability. The master equation can be solved by expressing the initial probability $\boldsymbol{P}^{(t=0)}$ as a linear combination of the left eigenvectors of the matrix R (see, e.g., [42, 45]), but this would take us too far off field. Instead, we wish to focus on the weak form of the dynamics, for which there are two crucial mathematical ingredients.

Our first ingredient is the inner product between two observables, $\mathcal{A}$ and $\mathcal{B}$ (i.e. two mappings from Ω to the real numbers). Let $\mathbb{E}^T[\mathcal{A}] = \sum_{\boldsymbol{x} \in \Omega} \pi_{\boldsymbol{x}}^T \mathcal{A}(\boldsymbol{x})$ be the equilibrium expected value of $\mathcal{A}$ at temperature T ($\pi_{\boldsymbol{x}}^T$ is the Boltzmann weight for state $\boldsymbol{x}$). The inner product of $\mathcal{A}$ and $\mathcal{B}$ is defined at the bath temperature:

$$\langle \mathcal{A} \,|\, \mathcal{B} \rangle := \mathbb{E}^{T_b}[\mathcal{A} \mathcal{B}] = \sum_{\boldsymbol{x} \in \Omega} \pi_{\boldsymbol{x}}^{T_b} \mathcal{A}(\boldsymbol{x}) \mathcal{B}(\boldsymbol{x}). \qquad (2)$$

In particular, let $\mathbf{1}$ be the constant observable such that $\mathbf{1}(\boldsymbol{x}) = 1$ for any state $\boldsymbol{x}$. Hence, for any observable

$\mathcal{A}$, $\langle \mathbf{1} \,|\, \mathcal{A} \rangle = \mathbb{E}^{T_b}[\mathcal{A}]$, while the equilibrium variance at temperature T_b is $\langle \mathcal{A}^\perp \,|\, \mathcal{A}^\perp \rangle$, where $\mathcal{A}^\perp := \mathcal{A} - \mathbf{1}\mathbb{E}^{T_b}[\mathcal{A}]$ accounts for the *fluctuations* of $\mathcal{A}$ from its expected value at T_b. Furthermore, the fluctuation-dissipation theorem tells us that

$$T^2 \left. \frac{\mathrm{d}\mathbb{E}^T[\mathcal{A}]}{\mathrm{d}T} \right|_{T=T_b} = \langle \mathcal{A}^\perp \,|\, \mathcal{E} \rangle \qquad (3)$$

($\mathcal{E}$ is the energy, and $\langle \mathcal{A}^\perp \,|\, \mathcal{E} \rangle = \mathbb{E}^T[\mathcal{A}\mathcal{E}] - \mathbb{E}^T[\mathcal{A}] \, \mathbb{E}^T[\mathcal{E}]$).

Our second crucial ingredient is the operator $\mathcal{R}$, that generates the time evolution of observables: $\mathcal{R}[\mathcal{A}](\boldsymbol{x}) = \sum_{\boldsymbol{y} \in \Omega} R_{\boldsymbol{x},\boldsymbol{y}} \mathcal{A}(\boldsymbol{y})$ [the matrix R was defined in Eq. (1)]. In particular, $\mathcal{R}[\mathbf{1}](\boldsymbol{x}) = 0$ for all $\boldsymbol{x}$ due to probability conservation (hence, $\mathbf{1}$ is an eigenfunction: $\mathcal{R}[\mathbf{1}] = 0 \cdot \mathbf{1}$).

Detailed balance implies that $\mathcal{R}$ is self-adjoint with respect to the inner product (2). For any $\mathcal{A}$ and $\mathcal{B}$

$$\langle \mathcal{R}[\mathcal{A}] \,|\, \mathcal{B} \rangle = \langle \mathcal{A} \,|\, \mathcal{R}[\mathcal{B}] \rangle. \qquad (4)$$

It follows that we can find an orthonormal basis of the space of observables with finite variance $(\mathbf{1}, \mathcal{O}_2^b, \mathcal{O}_3^b, \ldots)$, in which the $\mathcal{O}_k^b$ are all eigenfunctions $\mathcal{R}[\mathcal{O}_k^b] = \lambda_k \mathcal{O}_k^b$ [47]. We order the basis in such a way that $0 = \lambda_1 > \lambda_2 \geq \lambda_3 \geq \ldots$. Take now an arbitrary starting distribution function $\boldsymbol{P}^{(t=0)}$ at time $t = 0$. The expected value of *any* finite-variance observable $\mathcal{A}$ at time $t > 0$ is

$$\mathbb{E}_t[\mathcal{A}] = \mathbb{E}^{T_b}[\mathcal{A}] + \sum_{k \geq 2} \alpha_k^{(t=0)} \beta_k^{\mathcal{A}} \, \mathrm{e}^{-|\lambda_k| t/\tau_0}, \qquad (5)$$

$$\beta_k^{\mathcal{A}} = \langle \mathcal{O}_k^b \,|\, \mathcal{A} \rangle, \quad \alpha_k^{(t=0)} = \sum_{\boldsymbol{x} \in \Omega} P_{\boldsymbol{x}}^{(t=0)} \mathcal{O}_k^b(\boldsymbol{x}). \quad (6)$$

As long as the system shows separation of timescales (i.e. $|\lambda_2| < |\lambda_3|$), Eq. (5) gives rise to a hierarchy of physical magnitudes, with $\mathcal{O}_2^b$ having the slowest decay. If we are able to find an initial setup such that $\alpha_2^{(t=0)} = 0$—all $\alpha_k^{(t=0)}$ are independent of the observable $\mathcal{A}$ under consideration—then, provided that $\beta_2^{\mathcal{A}} \neq 0$, its expected value will benefit from an exponential speedup in the evolution toward its equilibrium value $\mathbb{E}^{T_b}[\mathcal{A}]$.

It is important to notice that the initial setup that will be used to speed up the system—coded in the starting probability $\boldsymbol{P}^{(t=0)}$—is not restricted to an equilibrium state. However, our interest lies on equilibrium states because they are easier to control (e.g., experimentally). For instance, using an equilibrium initial condition, the requirement for a speedup would be met if we can find a temperature $T \neq T_b$ such that $\alpha_2^{(t=0)} \equiv \mathbb{E}^T[\mathcal{O}_2^b] = 0$. We show below how to find (or force) this condition, explaining along the way different anomalous behaviors.

Experimental suitability. If the number of states is large enough, the spectral decomposition (5) might not be practical. In particular, the slowest decaying observable $\mathcal{O}_2^b$ might be unknown (or, even if known, its experimental measurement may present difficulties). Nonetheless, in some situations there may be a simple way out.

Specifically, let us consider the neighborhood of a first-order phase transition at zero temperature separating two ground states with different symmetries (we consider a specific example below). Let $\mathcal{M}_w$ be the order parameter of the unstable phase (the suffix w stands for *wrong*). If symmetries are such that $\mathbb{E}^T[\mathcal{M}_w] = 0$ for all T, then there are good chances that $(\mathcal{M}_w^2)^\perp$ will be a nice proxy for $\mathcal{O}_2^b$. Indeed, at phase coexistence, slow observable dynamics (OD) often stems from metastability [48]. We consider $(\mathcal{M}_w^2)^\perp$, the fluctuating part of $\mathcal{M}_w^2$, to mimic the behavior of $\mathcal{O}_2^b$: $0 = \langle \mathbf{1} \,|\, \mathcal{O}_2^b \rangle = \mathbb{E}^{T_b}[\mathcal{O}_2^b]$.

We expect $1 \approx \langle (\mathcal{M}_w^2)^\perp \,|\, \mathcal{O}_2^b \rangle / \langle (\mathcal{M}_w^2)^\perp \,|\, (\mathcal{M}_w^2)^\perp \rangle^{1/2}$ for any good proxy: in geometrical terms, the angle between $\mathcal{O}_2^b$ and $(\mathcal{M}_w^2)^\perp$ defined by the scalar product (2) will be small.

The crucial point leading to unconventional OD effects is that $\mathbb{E}^T[\mathcal{M}_w^2]$ is a *nonmonotonic function* of T, and we can find a bath temperature T_b^* such that $\mathrm{d}\,\mathbb{E}^T[\mathcal{M}_w^2]/\mathrm{d}T|_{T=T_b^*} = 0$ (see Figs. 1 and 2). This maximum generates surprising OD.

The behavior in Figs. 1 and 2 is generic because $\mathbb{E}^T[\mathcal{M}_w^2]$ is proportional to the susceptibility of $\mathcal{M}_w$ with respect to its conjugate field. Now, this susceptibility vanishes when $T \to 0$ (because $\mathcal{M}_w$ is the order parameter for the unstable phase) while, for large enough T, all susceptibilities decrease as T grows.

The basic observation. Consider the spectral decomposition (5) when the starting distribution $\boldsymbol{P}^{(t=0)}$ is the Boltzmann weight for some temperature $T^* \neq T_b$. We can approximate coefficient $\alpha_2^{(t=0)}$ as

$$\alpha_2^{(t=0)} \approx \frac{1}{\Lambda}\Big(\mathbb{E}^{T^*}[\mathcal{M}_w^2] \;-\; \mathbb{E}^{T_b}[\mathcal{M}_w^2] \Big), \qquad (7)$$

with $\Lambda = \langle (\mathcal{M}_w^2)^\perp \,|\, (\mathcal{M}_w^2)^\perp \rangle^{1/2}$ a relatively uninteresting constant fixed by the bath temperature [49]. In the more general case, $\mathbb{E}^{T^*}[\mathcal{M}_w^2]$ should be traded with $\mathbb{E}_{t=0}[\mathcal{M}_w^2]$ in Eq. (7). Several anomalous effects can be better understood from this simple observation.

The Markovian Mpemba effect [13]. Consider a bath at temperature T_b and two other temperatures, T_c and T_h such that $T_b < T_c < T_h$, chosen to have expected values of $\mathcal{M}_w^2$ as shown in Fig. 1(a). In the view of Eq. (7), it is clear that $\alpha_2^h = 0$, while $|\alpha_2^c| > 0$. This means that, provided that we start from a system in equilibrium at T_h, any observable $\mathcal{A}$ with $\beta_2^{\mathcal{A}} \neq 0$ [cf. Eq. (5)] will benefit from an exponential OD speedup, in its approach to equilibrium at T_b. Instead, the system originally in equilibrium at T_c will display a slower relaxation in the bath at T_b. This is regarded as the strong ME [14]. Mind that, in general, T_h will not be such that $\mathbb{E}^{T_h}[\mathcal{M}_w^2]$ exactly equals $\mathbb{E}^{T_b}[\mathcal{M}_w^2]$, but T_h will be near the temperature where exact equality is achieved. That is, the condition $0 < |\alpha_2^h| < |\alpha_2^c|$ is fulfilled, which leads to a subexponential speedup regarded as the weak ME [14].

In particular, the ME will be most spectacular if we choose $\mathcal{A}$ such that $\mathbb{E}^{T_c}[\mathcal{A}]$ is closer to $\mathbb{E}^{T_b}[\mathcal{A}]$ than $\mathbb{E}^{T_h}[\mathcal{A}]$
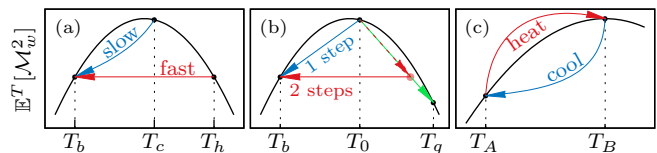

FIG. 1. Staging the anomalous effects. (a) The Mpemba effect. (b) Preheating for faster cooling. (c) Asymmetry of heating and cooling processes.

is, because in that case the difference $\mathbb{E}_t^h[\mathcal{A}] - \mathbb{E}_t^c[\mathcal{A}]$ will change sign in a clearer way.

Preheating for faster cooling. In these protocols [29, 30] the transition of the system from equilibrium at temperature T_0 toward equilibrium at bath temperature $T_b < T_0$ can be done faster by introducing a brief sudden quench at a higher temperature $T_q > T_0$, rather than simply leaving the system to freely relax under the action of the bath.

In order to amplify the effect, we choose T_0 near the maximum of $\mathbb{E}^T[\mathcal{M}_w^2]$, so that $\alpha_2^{T_0 \to T_b}$ will be as large as possible, cf. Eq. (7). On the other hand, we choose $T_q \gg T_0$ so that $\mathbb{E}^{T_b}[\mathcal{M}_w^2] > \mathbb{E}^{T_q}[\mathcal{M}_w^2]$, see Fig. 1(b). Now, starting from the equilibrated system at T_0, we instantaneously raise the bath temperature to T_q, and let the system relax. During the relaxation, the expected value of $\mathcal{M}_w^2$ decreases from its initial value (which is the T_0 equilibrium value) and eventually crosses $\mathbb{E}^{T_b}[\mathcal{M}_w^2]$ at a time t'. This means [cf. Eq. (7)] that we can find a suitable time $t_w \approx t'$ such that, if we instantaneously lower the bath temperature from T_q to T_b at time t_w, we shall start the relaxation at T_b with $\alpha_2^{t_w} = 0$. The t_w time overhead, due to the initial temperature excursion from T_0 to T_q, is compensated by the exponential speedup at T_b, that would otherwise be absent.

Heating and cooling may be asymmetric processes (see also [37, 38]). Let us consider the maximum of $\mathbb{E}^T[\mathcal{M}_w^2]$ at $T = T_b^*$ in Fig. 1(c). Given the aforementioned relation between metastability and slow relaxations, it is natural to expect that the largest relaxation time in the system $1/|\lambda_2|$, see Eq. (5), will also attain its maximum value at T_b^* (the asymmetry stems from λ_2, rather than α_2). Now, one would naively think taking to equilibrium at T_A a system initially at equilibrium at T_B would take the same time as the inverse process $T_A \to T_B$. Quite on the contrary, if we choose $T_B = T_b^*$ the process $T_B \to T_A$ is *faster* than its counterpart $T_A \to T_B$, no matter whether $T_A < T_B$ or $T_A > T_B$. Indeed, Eq. (7) tells us that $\alpha_2^{T_B \to T_A}$ and $\alpha_2^{T_A \to T_B}$ are numbers of similar magnitude (but opposite sign). Hence, the slowness of the relaxation is ruled by $1/|\lambda_2|$, which is larger at T_B.

The relaxation of the energy is an important exception, however. Indeed, applying Eq. (3) to $\mathcal{M}_w^2$, one finds that $\beta_2^{\mathcal{E}}$ [cf. Eq. (5)] is inordinately small at $T_B = T_b^*$. There-

fore, the approach to equilibrium of $\mathcal{E}$ at T_B is ruled by λ_3 rather than λ_2, which precludes us from making definite predictions.

A working example: The antiferromagnetic 1D Ising model. We consider a periodic chain with N spins $\sigma_i = \pm 1$, $1 \leq i \leq N$, and $\sigma_{N+1} := \sigma_1$. The state space is given by $\Omega = \{-1, 1\}^N$. The energy for a given spin configuration $\boldsymbol{x} = (\sigma_1, \sigma_2, \ldots, \sigma_N)$ is

$$\mathcal{E}(\boldsymbol{x}) := -J \sum_{k=1}^{N} \sigma_k \, \sigma_{k+1} - h \sum_{k=1}^{N} \sigma_k \,, \qquad (8)$$

where we assume $J < 0$ and $h > 0$, as well as N even to avoid frustration. The minimum energy configuration differs at both sides of the line $2J + h = 0$. If $J > -h/2$ the ground state (GS) is the uniform configuration $\{\sigma_i = 1\}$. Instead, if $J < -h/2$ the GS is one of the two AF ordered staggered configurations $\{\sigma_i = (-1)^i\}$ or $\{\sigma_i = (-1)^{i+1}\}$. Therefore, the first-order transition at $T = 0$ needed to demonstrate exotic OD is realized in this model.

The uniform ($\mathcal{M}_u$) and the staggered ($\mathcal{M}_{\mathrm{st}}$) magnetizations are order parameters able to discriminate our GS:

$$\mathcal{M}_u(\boldsymbol{x}) = \sum_{k=1}^{N} \sigma_k \,, \quad \mathcal{M}_{\mathrm{st}}(\boldsymbol{x}) = \sum_{k=1}^{N} (-1)^k \sigma_k \qquad (9)$$

(for the uniform GS, $\mathcal{M}_u = N$ and $\mathcal{M}_{\mathrm{st}} = 0$, while for the staggered GSs one finds $\mathcal{M}_u = 0$ and $\mathcal{M}_{\mathrm{st}} = \pm N$). The energy $\mathcal{E}$ (8) is invariant under spatial translations ($\sigma_i \to \sigma_{i+1}$) which ensures that $\mathbb{E}^T[\mathcal{M}_{\mathrm{st}}] = 0$ for all temperatures. This is why we make stable the uniform GS by choosing $(J, h) = (-4, 8.2)$. Hence, our *wrong* order parameter will be $\mathcal{M}_w \equiv \mathcal{M}_{\mathrm{st}}$.

Other magnitudes of interest will be the staggered susceptibility χ_{st} and the spin-spin interaction $\mathcal{C}_1$:

$$\chi_{\mathrm{st}} = \frac{1}{N} \, \mathbb{E}^T[\mathcal{M}_{\mathrm{st}}^2] \,, \quad \mathcal{C}_1(\boldsymbol{x}) = \sum_{k=1}^{N} \sigma_k \, \sigma_{k+1} \,. \qquad (10)$$

The reader will note that all our magnitudes of interest (namely, $\mathcal{M}_u$, $\mathcal{M}_{\mathrm{st}}^2$, $\mathcal{E}$, and $\mathcal{C}_1$) are invariant under spatial translations. Also our dynamics, see Eq. (1), preserves the translation invariance of the starting probability $\boldsymbol{P}^{(t=0)}$. Hence, the spectral decomposition (5) can be restricted to the subspace of magnitudes $\mathcal{O}_k^b$ that are themselves invariant under translations.

Figure 2 shows that the two conditions necessary for exotic OD [namely, a nonmonotonic behavior of χ_{st} and a small angle—as defined by Eq. (2)—between $(\mathcal{M}_{\mathrm{st}}^2)^\perp$ and $\mathcal{O}_2^b$] are met with our working parameters.

Results. We have considered the three protocols explained in Fig. 1 in the 1D AF Ising model considered above. We have studied a single-site dynamics (heat-bath dynamics or Gibbs sampler [42, 43, 45]). For short
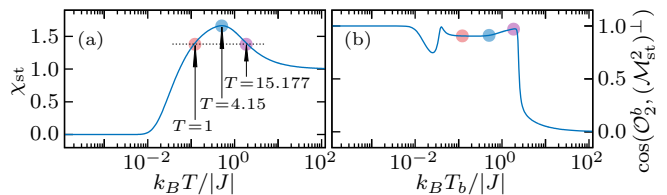

FIG. 2. Validation of $(\mathcal{M}_{\mathrm{st}}^2)^\perp$ as a proxy for the slowest decaying observable $\mathcal{O}_2^b$. (a) χ_{st} as computed for $N \to \infty$ vs. $k_B T/|J|$, see Eq. (10), has a maximum at $T_b^* \approx 4.15$. The curves for $N = 8$ and $N \to \infty$ are hardly distinguishable at this scale. (b) For $N = 8$, the cosine of the angle between $(\mathcal{M}_{\mathrm{st}}^2)^\perp$ and $\mathcal{O}_2^b$ is close to 1 for a wide range of bath temperatures. The colored dots in (a) and (b) indicate the three temperatures that we mostly use to demonstrate unconventional OD.

chains ($N = 8, 12$), we solved the master equation (1) through Monte Carlo (MC) simulations, and by finding the "exact" spectral decomposition of the operator R [50], full details can be found in [45]. The two methods were in full agreement and supported the proposed approach for small $N = 8, 12$. For larger chains ($N = 32$), only MC simulations were computationally feasible and, again, validated our proposal. For clarity's sake, we only show numerical results for a selection observables (see [45] for the remaining ones). In all three protocols, we have found statistically compatible results for $N = 12$ and 32.

Figure 3 illustrates the ME as obtained with $T_b = 1$, $T_c = 4.15$, and $T_h = 15.177$, by a change of sign in

$$\Delta_t[\mathcal{A}] := \frac{1}{N} \left(\mathbb{E}_t^h[\mathcal{A}] - \mathbb{E}_t^c[\mathcal{A}] \right) \,. \qquad (11)$$
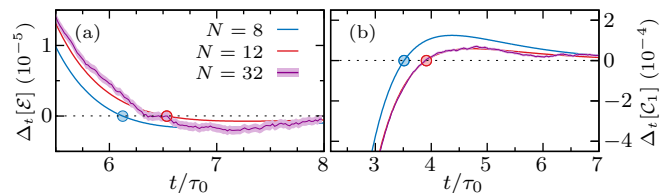

FIG. 3. Mpemba effect. Evolution of $\Delta_t[\mathcal{A}]$ [cf. Eq. (11)] for the observables $\mathcal{A} = \mathcal{E}$ (a), and $\mathcal{A} = \mathcal{C}_1$ (b). We show the results for $N = 8$ (blue), $N = 12$ (red), and $N = 32$ (purple, with a lighter shade representing the error bars of the MC data). The time at which $\Delta_t[\mathcal{A}]$ changes sign is marked by a dot.

Supercooling through preheating is illustrated in Fig. 4, with the choices $T_b = 1$, $T_0 = 4.15$, $T_q = 2000$ and $t_w = 0.156$. It is useful to define

$$\delta_t[\mathcal{A}] := \frac{1}{N} \left| \mathbb{E}_t[\mathcal{A}] - \mathbb{E}^{T_b}[\mathcal{A}] \right| \,. \qquad (12)$$

Finally, the asymmetry between heating and cooling is illustrated in Fig. 5(a) with the choices $T_A = 1$ and $T_B =$
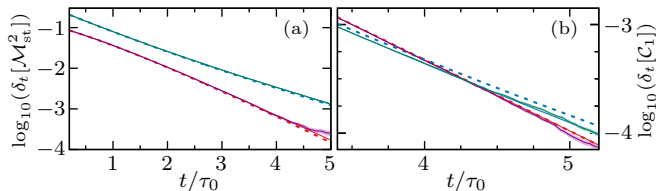
FIG. 4. Preheating strategy for faster cooling. Evolution of $\delta_t[\mathcal{A}]$ [cf. Eq. (12)] for $\mathcal{A} = \mathcal{M}_{st}^2$ (a), and $\mathcal{A} = \mathcal{C}_1$ (b). Colors red and purple (respectively, blue and green) denote that the protocol includes (respectively does not include) an initial quench at temperature T_q. We show data for $N = 8$ (dashed lines), $N = 12$ (solid lines), and $N = 32$ (solid lines with a lighter shade representing the error bars of the MC data). Both panels show the expected speedup for the preheating protocol.

$4.15 \approx T_b^*$, and in Fig. 5(b) with the choices $T_A = 15.177$ and $T_B = 4.15$.
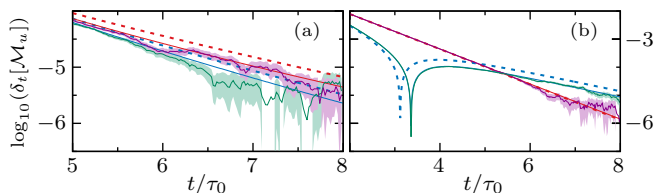

FIG. 5. (A)symmetry in heating and cooling. Evolution of $\delta_t[\mathcal{M}_u]$ [cf. Eq. (12)] for cooling (blue and green) and heating (red and purple) processes. We show data for $N = 8$ (dashed lines), $N = 12$ (solid lines), and $N = 32$ (solid lines with a lighter shade representing the errors of the MC data). The cooling and heating processes were carried out between: (a) $T_A = 1$ and $T_B = 4.15$; and (b) $T_A = 15.177$ and $T_B = 4.15$. Note that in panel (b), $\mathbb{E}_t[\mathcal{M}_u] - \mathbb{E}^{T_b = T_B}[\mathcal{M}_u]$ changes sign at $t \approx 3$ for the system originally at $T_A = 15.177$. It is always slower to approach $T_B = 4.15$: i.e. to heat up in (a), and to cool down in (b).

Discussion. We have shown that the "weak form" of Markov dynamics provides a unified, geometric framework that allows us to explain and control several exotic OD effects pertaining to the Mpemba effect realm. Our approach departs from previous work that usually privilege the "strong form" of the dynamics by following the evolution of the system entropy (or, rather, some kind of entropic "distance" such as the Kullback-Leibler divergence [51]). We have dealt, instead, with different physical observables, some of which can be measured at the mesoscopic level. Our geometric approach has unearthed an orthogonality phenomenon that may cause an observable as prominent as the energy to remain blind to the overall speedup achieved by the temperature changing protocols. This result warns that one cannot have a too-narrow spectrum of observables when investigating the Mpemba effect [52, 53].

Finite-size effects on the separation of timescales are also of concern, because it is this separation what de-termines the attainable exponential speedup. Fortunately, we have found that the speedup depends very mildly (if at all) on the system size. Finally, we stress that the approach presented here can also be applied to other systems where anomalous relaxation has been observed [15, 29, 38], and where the nonmonotonicity of equilibrium thermodynamic observables is also present. Also, extending our approach to the analysis of the time-varying temperature protocols followed in recent experiments [54] is an exciting venue for future work.

* Corresponding author: alasanta@ugr.es
[1] H. Nyquist, Phys. Rev. **32**, 110 (1928).
[2] R. Zwanzig, Annu. Rev. Phys. Chem. **16**, 67 (1965).
[3] L. Onsager, Phys. Rev. **37**, 405 (1931).
[4] L. Onsager, Phys. Rev. **38**, 2265 (1931).
[5] R. Kubo, Rep. Prog. Phys. **29**, 255 (1966).
[6] U. M. B. Marconi, A. Puglisi, L. Rondoni, and A. Vulpiani, Phys. Rep. **461**, 111 (2008), arXiv:0803.0719.
[7] D. J. Evans, D. J. Searles, and S. R. Williams, J. Chem. Phys. **128**, 014504 (2008).
[8] D. J. Evans, D. J. Searles, and S. R. Williams, J. Chem. Phys. **128**, 249901 (2008).
[9] U. Seifert, Rep. Prog. Phys. **75**, 126001 (2012), arXiv:1205.4176.
[10] M. Jeng, Am. J. Phys. **74**, 514 (2006), arXiv:physics/0512262.
[11] E. B. Mpemba and D. G. Osborne, Phys. Educ. **4**, 172

(1969).

[12] J. Bechhoefer, A. Kumar, and R. Chétrite, Nat. Rev. Phys. **3**, 534 (2021).

[13] Z. Lu and O. Raz, Proc. Natl. Acad. Sci. U.S.A. **114**, 5083 (2017), arXiv:1609.05271.

[14] I. Klich, O. Raz, O. Hirschberg, and M. Vucelja, Phys. Rev. X **9**, 021060 (2019), arXiv:1711.05829.

[15] A. Kumar and J. Bechhoefer, Nature (London) **584**, 64 (2020), arXiv:2008.02373.

[16] M. R. Walker and M. Vucelja, J. Stat. Mech. **2021**, 113105 (2021), arXiv:2105.10656.

[17] A. Biswas, R. Rajesh, and A. Pal, J. Chem. Phys. **159**, 044120 (2023), arXiv:2304.06420.

[18] F. J. Schwarzendahl and H. Löwen, Phys. Rev. Lett. **129**, 138002 (2022), arXiv:2111.06109.

[19] A. Kumar, R. Chétrite, and J. Bechhoefer, Proc. Natl. Acad. Sci. U.S.A. **119**, 2118484119 (2022), arXiv:2104.12899.

[20] N. Vadakkayil and S. K. Das, Phys. Chem. Chem. Phys. **23**, 11186 (2021), arXiv:2210.02727.

[21] F. Carollo, A. Lasanta, and I. Lesanovsky, Phys. Rev. Lett. **127**, 060401 (2021), arXiv:2103.05020.

[22] A. Nava and M. Fabrizio, Phys. Rev. B **100**, 125102 (2019), arXiv:1905.12029.

[23] A. K. Chatterjee, S. Takada, and H. Hayakawa, Phys. Rev. Lett. **131**, 080402 (2023), arXiv:2304.02411.

[24] A. Gijón, A. Lasanta, and E. R. Hernández, Phys. Rev. E **100**, 032103 (2019), arXiv:1906.10813.

[25] A. Lasanta, F. Vega Reyes, A. Prados, and A. Santos, Phys. Rev. Lett. **119**, 148001 (2017), arXiv:1611.04948.

[26] A. Torrente, M. A. López-Castaño, A. Lasanta, F. Vega Reyes, A. Prados, and A. Santos, Phys. Rev. E **99**, 060901(R) (2019), arXiv:1902.09404.

[27] E. Mompó, M. A. López-Castaño, A. Lasanta, F. Vega Reyes, and A. Torrente, Phys. Fluids **33**, 062005 (2021), arXiv:1902.09404.

[28] M. Baity-Jesi, E. Calore, A. Cruz, L. A. Fernández, J. M. Gil-Narvión, A. Gordillo-Guerrero, D. Íñiguez, A. Lasanta, A. Maiorano, E. Marinari, V. Martín-Mayor, J. Moreno-Gordo, A. Muñoz Sudupe, D. Navarro, G. Parisi, S. Pérez-Gaviro, F. Ricci-Tersenghi, J. J. Ruiz-Lorenzo, S. F. Schifano, B. Seoane, A. Tarancón, R. Tripiccione, and D. Yllanes, Proc. Natl. Acad. Sci. U.S.A. **116**, 15350 (2019), arXiv:1804.07569.

[29] A. Gal and O. Raz, Phys. Rev. Lett. **124**, 060602 (2020), arXiv:1909.06113.

[30] I. G.-A. Pemartín, E. Mompó, A. Lasanta, V. Martín-Mayor, and J. Salas, Phys. Rev. E **104**, 044114 (2021), arXiv:2105.13973.

[31] D. Guéry-Odelin, C. Jarzynski, C. A. Plata, A. Prados, and E. Trizac, Rep. Prog. Phys. **86**, 035902 (2023), arXiv:2204.11102.

[32] S. S. Chittari and Z. Lu, J. Chem. Phys. **159**, 084106 (2023), arXiv:2304.06822.

[33] A. J. Kovacs, Fortschr. Hochpolym. Forsch. **3**, 394 (1964).

[34] A. J. Kovacs, J. J. Aklonis, J. M. Hutchinson, and A. R. Ramos, J. Polym. Sci. Pol. Phys. **17**, 1097 (1979).

[35] A. Prados and E. Trizac, Phys. Rev. Lett. **112**, 198001 (2014), arXiv:1404.6162.

[36] A. Militaru, A. Lasanta, M. Frimmer, L. L. Bonilla, L. Novotny, and R. A. Rica, Phys. Rev. Lett. **127**, 130603 (2021), arXiv:2103.14412.

[37] A. Lapolla and A. Godec, Phys. Rev. Lett. **125**, 110602 (2020), arXiv:2002.08237.

[38] M. Ibáñez, C. Dieball, A. Lasanta, A. Godec, and R. A. Rica, Nat. Phys. **20**, 135 (2024), arXiv:2302.09061.

[39] G. E. Crooks, Phys. Rev. Lett. **99**, 100602 (2007), arXiv:0706.0559.

[40] S. Ito and A. Dechant, Phys. Rev. X **10**, 021056 (2020), arXiv:1810.06832.

[41] U. Wolff, Phys. Rev. Lett. **62**, 361 (1989).

[42] D. A. Levin and Y. Peres, *Markov Chains and Mixing Times*, Vol. 107 (American Mathematical Soc., Providence, 2017).

[43] A. D. Sokal, *In Functional Integration: Basics and Applications (1996 Cargèse School)*, edited by C. DeWitt-Morette, P. Cartier, and A. Folacci (Plenum, New York, 1997).

[44] These two viewpoints remind the Heisenberg and Schrödinger pictures of time evolution in quantum mechanics.

[45] See Supplemental Material, at http://link.aps.org/supplemental/10.1103/PhysRevLett.132.117102 for a short description of the weak and strong forms of Markov dynamics, the connection between discrete-time and continuous-time Markov Chain Monte Carlo, simulation details, and additional results, which includes Refs. [55, 56].

[46] For a chain of N Ising spins, the number of states is $|\Omega| = 2^N$. For $|\Omega| = \infty$, the natural mathematical framework is functional analysis (rather than linear algebra).

[47] Superscripts b are twofold. They stress the fact that the observables $\mathcal{O}_k^b$ are tied to the bath temperature T_b, and that detailed balance, Eq. (4), is only fulfilled for the scalar product at temperature T_b.

[48] G. Parisi, *Statistical Field Theory* (Addison-Wesley, 1988).

[49] Recall that $(\mathcal{M}_w^2)^\perp = \mathcal{M}_w^2 - \mathbf{1}\mathbb{E}^{T_b}[\mathcal{M}_w^2]$ mimics $\mathcal{O}_2^b$ in the sense that $\mathbb{E}^{T_b}[\mathcal{O}_2^b] = 0$. After accounting for normalization, $\alpha_2^{(t=0)} \approx \Lambda^{-1} \mathbb{E}^{T_b}[(\mathcal{M}_w^2)^\perp]$, which leads to Eq. (7).

[50] Strictly speaking, we computed the spectral decomposition of R using 300-digit arithmetic [45].

[51] S. Kullback and R. A. Leibler, Ann. Math. Statist. **22**, 79 (1951).

[52] A. Biswas, V. V. Prasad, and R. Rajesh, Phys. Rev. E **108**, 024902 (2023), arXiv:2303.10900.

[53] A. Megías, A. Santos, and A. Prados, Phys. Rev. E **105**, 054140 (2022), arXiv:2201.13130.

[54] L. B. Pires, R. Goerlich, A. L. da Fonseca, M. Debiossac, P.-A. Hervieux, G. Manfredi, and C. Genet, Phys. Rev. Lett. **131**, 097101 (2023), arXiv:2302.06003.

[55] A. B. Bortz, M. H. Kalos, and J. L. Lebowitz, J. Comp. Phys. **17**, 10 (1975).

[56] D. T. Gillespie, J. Phys. Chem. **81**, 2340 (1977).

Supplemental Material for "Shortcuts of freely relaxing systems using equilibrium physical observables"

Isidoro González-Adalid Pemartín,[1] Emanuel Mompó,[2, 3] Antonio
Lasanta,[4, 5, *] Víctor Martín-Mayor,[1, 6] and Jesús Salas[7, 8]

[1]*Departamento de Física Teórica, Universidad Complutense, 28040 Madrid, Spain*
[2]*Departamento de Matemática Aplicada, Grupo de Dinámica No Lineal,
Universidad Pontificia Comillas, Alberto Aguilera 25, 28015 Madrid, Spain*
[3]*Instituto de Investigación Tecnológica (IIT), Universidad Pontificia Comillas, 28015 Madrid, Spain*
[4]*Departamento de Álgebra, Facultad de Educación, Economía y Tecnología de Ceuta,
Universidad de Granada, Cortadura del Valle, s/n, 51001 Ceuta, Spain*
[5]*Nanoparticles Trapping Laboratory, Universidad de Granada, Granada, Spain*
[6]*Instituto de Biocomputación y Física de Sistemas Complejos (BIFI), 50018 Zaragoza, Spain*
[7]*Departamento de Matemáticas, Universidad Carlos III de Madrid, 28911 Leganés, Spain*
[8]*Grupo de Teorías de Campos y Física Estadística,
Instituto Gregorio Millán, Universidad Carlos III de Madrid,
Unidad Asociada al Instituto de Estructura de la Materia, CSIC, Spain*
(Dated: August 9, 2023)

In this Supplemental Material we will give extra details about our work. In Sec. I, we will discuss the Markov dynamics, as well as the ways we have implemented it. In Sec. II, we will display exact formulae related to some expectation values of interest for a 1D Ising model in an external magnetic field. Finally, in Sec. III, we show some additional results that could not be displayed in the main text for lack of space.

I. THE MARKOV DYNAMICS

In order to explain our continuous-time dynamics, we shall follow this step-by-step approach:

1. We shall recall in Sec. I A the necessary mathematical ideas in the familiar context of discrete-time Markov Chain Monte Carlo (MC); for a more paused exposition see e.g. Refs. [1, 2].

2. We show in Sec. I B how to obtain a lazy version of any discrete-time Markov chain, emphasizing how the basic formulae need to be modified for the lazy version of the dynamics. [3]

3. The continuous-time Markov dynamics is straightforwardly obtained from the lazy discrete-time algorithm as explained in Sec. I C.

4. Finally, we recall in Sec. I D how the *n*-fold way idea [4, 5] allows us to obtain a rejection-free algorithm for our Markov dynamics with continuous time.

In order to give some flesh to the general formulae, we shall use the example of the Ising spin chain that is studied in the main text. The inner product between *real* observables will also be defined here as in the main text [6]:

$$\langle \mathcal{A} \,|\, \mathcal{B} \rangle \;:=\; \sum_{\boldsymbol{x}\in\Omega} \pi_{\boldsymbol{x}}^{T_b} \, \mathcal{A}(\boldsymbol{x}) \, \mathcal{B}(\boldsymbol{x}) \,. \tag{1}$$

Indeed, whether the dynamics are discrete or continuous time does not make any difference in this respect.

Specifically, in examples we shall be referring to a periodic chain with N spins $\sigma_i = \pm 1$, $1 \le i \le N$. The state space is given by $\Omega = \{-1, 1\}^N$. Hence, the number of states is $|\Omega| = 2^N$. The energy for a given spin configuration $\boldsymbol{x} = (\sigma_1, \sigma_2, \ldots, \sigma_N)$ is

$$\mathcal{E}(\boldsymbol{x}) \;:=\; -J\sum_{k=1}^{N} \sigma_k\,\sigma_{k+1} - h\sum_{k=1}^{N} \sigma_k \,, \tag{2}$$

where we assume $\sigma_{N+1} := \sigma_1$ due to the periodic boundary conditions. The chain length will be even, so there is no frustration in the antiferromagnetic regime (i.e., $J < 0$).

The partition function of this model is given by $Z_N(J, h; T_b) = \sum_{\boldsymbol{x}\in\Omega} \exp\{-\mathcal{E}(\boldsymbol{x})/(k_B T_b)\}$, making

$$\pi_{\boldsymbol{x}}^{T_b}(J, h) \;=\; \frac{\exp\{-\mathcal{E}(\boldsymbol{x})/(k_B T_b)\}}{Z_N(J, h; T_b)} \tag{3}$$

to be the Boltzmann distribution $\boldsymbol{\pi}^{T_b}$ for the couplings (J, h) and the bath temperature T_b.

The main examples of observables that we shall be considering are the energy $\mathcal{E}$ (2), the uniform and staggered magnetizations

$$\mathcal{M}_{\mathrm{u}}(\boldsymbol{x}) = \sum_{k=1}^{N} \sigma_k \,, \quad \mathcal{M}_{\mathrm{st}}(\boldsymbol{x}) = \sum_{k=1}^{N} (-1)^k \sigma_k \,, \tag{4}$$

as well as the spin-spin interaction,

$$\mathcal{C}_1(\boldsymbol{x}) = \sum_{k=1}^{N} \sigma_k\,\sigma_{k+1} \,. \tag{5}$$

* Corresponding author: alasanta@ugr.es

From these observables we compute the following expectation values: the energy density $E = \mathbb{E}^T[\mathcal{E}]/N$, the uniform magnetization density $M_u = \mathbb{E}^T[\mathcal{M}_u]/N$, the spin-spin interaction $C_1 = \mathbb{E}^T[\mathcal{C}_1]/N$, and the staggered susceptibility $\chi_{\text{st}} = \mathbb{E}^T[\mathcal{M}_{\text{st}}^2]/N$. Note that the translation symmetry of the spin chain implies that $\mathbb{E}^T[\mathcal{M}_{\text{st}}] = 0$. Besides, as in the main text, here $\mathbf{1}$ is the constant function such that $\mathbf{1}(\boldsymbol{x}) = 1$ for any state $\boldsymbol{x}$.

A. Discrete time

Let $T_{\boldsymbol{x},\boldsymbol{y}}$ be the probability for the system to jump from state $\boldsymbol{x}$ to state $\boldsymbol{y}$ in a single time-step. If the number of states $|\Omega|$ is finite, $T_{\boldsymbol{x},\boldsymbol{y}}$ can be regarded as an element of an $|\Omega| \times |\Omega|$ matrix T.

The Markov and stationary properties of the dynamics are encoded in the so-called master equation. Let us denote $P_{\boldsymbol{x}}^{(m)}$ the probability of finding the system in state $\boldsymbol{x}$ at the discrete time-step m. Then, the probability after n further time-steps is

$$P_{\boldsymbol{y}}^{(m+n)} = \sum_{\boldsymbol{x} \in \Omega} P_{\boldsymbol{x}}^{(m)}[T^n]_{\boldsymbol{x},\boldsymbol{y}}, \tag{6}$$

where T^n is the n-th power of matrix T. In particular, we have the time evolution of the probability from the initial condition $P_{\boldsymbol{x}}^{(n=0)}$:

$$P_{\boldsymbol{y}}^{(n)} = \sum_{\boldsymbol{x} \in \Omega} P_{\boldsymbol{x}}^{(n=0)}[T^n]_{\boldsymbol{x},\boldsymbol{y}}, \tag{7}$$

Mind that, in this formalism, probabilities are regarded as row vectors that are right-multiplied by matrix T to get a new probability (hence, a new row vector).

The main properties that T should fulfill are positivity and completeness of the conditional probabilities,

$$T_{\boldsymbol{x},\boldsymbol{y}} \geq 0, \, \forall \boldsymbol{x}, \boldsymbol{y} \in \Omega; \quad \sum_{\boldsymbol{y} \in \Omega} T_{\boldsymbol{x},\boldsymbol{y}} = 1, \, \forall \boldsymbol{x} \in \Omega, \tag{8}$$

stationary,

$$\pi_{\boldsymbol{y}}^{T_b} = \sum_{\boldsymbol{y} \in \Omega} \pi_{\boldsymbol{x}}^{T_b} T_{\boldsymbol{x},\boldsymbol{y}}, \tag{9}$$

and irreducibility,

$$\forall \boldsymbol{x}, \boldsymbol{y} \in \Omega, \exists n_{\boldsymbol{x},\boldsymbol{y}} > 0 \text{ such that } [T^{n_{\boldsymbol{x},\boldsymbol{y}}}]_{\boldsymbol{x},\boldsymbol{y}} > 0. \tag{10}$$

Note that the stationary condition implies that the Boltzmann weight $\boldsymbol{\pi}^{T_b}$ is a left eigenvector of the matrix T, so that a system initially in thermal equilibrium at temperature T_b—i.e., distributed according to $\boldsymbol{\pi}^{T_b}$—remains in equilibrium forever, see Eq. (7). Irreducibility means that any state of the phase space Ω should be eventually reachable from any starting state $\boldsymbol{x}$.

Just to make one example, let us consider the Ising spin chain. The corresponding heat-bath discrete-time dynamics with random-access to the chain is encoded in the following way. If two, or more, spins take different values in configurations $\boldsymbol{x}$ and $\boldsymbol{y}$, then $T_{\boldsymbol{x},\boldsymbol{y}} = 0$. This is why this dynamic is sometimes described as single spin-flip. If $\boldsymbol{x}$ and $\boldsymbol{y}$ differ in the value of just one spin, then

$$T_{\boldsymbol{x},\boldsymbol{y}} = \frac{1}{N} R_{\boldsymbol{x},\boldsymbol{y}}^{\text{HB}}, \tag{11}$$

$$R_{\boldsymbol{x},\boldsymbol{y}}^{\text{HB}} = \frac{\exp\left\{-[\mathcal{E}(\boldsymbol{y}) - \mathcal{E}(\boldsymbol{x})]/(k_B T_b)\right\}}{1 + \exp\left\{-[\mathcal{E}(\boldsymbol{y}) - \mathcal{E}(\boldsymbol{x})]/(k_B T_b)\right\}}. \tag{12}$$

[Diagonal matrix elements $T_{\boldsymbol{x},\boldsymbol{x}}$ are fixed by the completeness condition (8)]. Mind that matrix T is very sparse: every row contains 2^N matrix elements, but only $N + 1$ of them are different from zero (i.e., the diagonal term, and the N states $\boldsymbol{y}$ that are connected with $\boldsymbol{x}$ by a single spin flip). In fact, the $1/N$ prefactor in Eq. (11) tells us that the spin that will be attempted to flip is chosen with uniform probability. The probability of accepting the spin-flip $R_{\boldsymbol{x},\boldsymbol{y}}^{\text{HB}}$ ensures that T verifies the detailed balance condition

$$\pi_{\boldsymbol{x}}^{T_b} T_{\boldsymbol{x},\boldsymbol{y}} = \pi_{\boldsymbol{y}}^{T_b} T_{\boldsymbol{y},\boldsymbol{x}}, \tag{13}$$

that can be straightforwardly combined with the completeness condition to show that detailed balance implies stationary (9) [7]. Showing that heat-bath verifies the other conditions (positivity, completeness, and irreducibility for positive temperature) is a textbook exercise.

Note as well that for single spin-flip dynamics it is customary to restrict the n in Eq. (7) to a multiple of N,

$$n = kN, \quad k \in \mathbb{N}, \tag{14}$$

so that every spin has (on average) k opportunities to be flipped.

At this point, it would be natural to solve Eq. (7) by finding a basis of left eigenvectors. However, it will prove useful to diagonalize instead the related operator $\mathcal{T}$ [8]. Given an observable $\mathcal{A}$, we obtain a new observable $\mathcal{T}[\mathcal{A}]$ as

$$\mathcal{T}[\mathcal{A}](\boldsymbol{x}) = \sum_{\boldsymbol{y} \in \Omega} T_{\boldsymbol{x},\boldsymbol{y}} \mathcal{A}(\boldsymbol{y}). \tag{15}$$

So, in this formalism, observables are identified with column vectors that are left-multiplied by the matrix T to get a new column vector, hence a new observable. The interpretation of the new observable $\mathcal{T}^n[\mathcal{A}]$ is simple: take a system initially in state $\boldsymbol{x}$, then $\mathcal{T}^n[\mathcal{A}](\boldsymbol{x})$ is the expected value of $\mathcal{A}$ after n dynamical steps [9]. The completeness condition implies as well that $\mathcal{T}[\mathbf{1}] = \mathbf{1}$ (i.e., $\mathbf{1}$ is a right eigenvector of $\mathcal{T}$ with eigenvalue one).

Now, the crucial observation is that, as the reader can easily show, detailed balance implies that $\mathcal{T}$ is a self-adjoint operator for the inner-product (1),

$$\langle \mathcal{T}[\mathcal{A}] | \mathcal{B} \rangle = \langle \mathcal{A} | \mathcal{T}[\mathcal{B}] \rangle. \tag{16}$$

It follows that the spectrum of $\mathcal{T}$ (and hence of T) is real. In addition, it follows from the completeness condition (8) that all eigenvalues belong to the interval $[-1, 1]$ (hence, the eigenvalue for the constant functions, $\Lambda_1 = 1$, is the largest one). Furthermore, one can find an orthogonal basis of right eigenvectors—orthogonal with respect to the inner product (1)—$(\mathbf{1}, \mathcal{O}_2^b, \mathcal{O}_3^b, \ldots)$:

$$\mathcal{T}[\mathcal{O}_k^b] = \Lambda_k \mathcal{O}_k^b, \tag{17}$$

$$1 = \Lambda_1 \geq \Lambda_2 \geq \Lambda_3 \geq \ldots \geq \Lambda_{|\Omega|} \geq -1. \tag{18}$$

One has a corresponding basis of left eigenvectors in which the starting probability can be linearly expressed ($\boldsymbol{v}_1 = \boldsymbol{\pi}^{T_b}$, of course)

$$\boldsymbol{v}_k T = \Lambda_k \boldsymbol{v}_k, \quad \boldsymbol{P}^{(n=0)} = \boldsymbol{\pi}^{T_b} + \sum_{k=2}^{|\Omega|} \gamma_k \boldsymbol{v}_k. \tag{19}$$

Hence, the dynamic evolution for the probability is

$$\boldsymbol{P}^{(n)} = \boldsymbol{\pi}^{T_b} + \sum_{k \geq 2} \Lambda_k^n \gamma_k \boldsymbol{v}_k, \tag{20}$$

while the discrete-time evolution for the expectation value of an arbitrary (finite-variance) magnitude $\mathcal{A}$ is

$$\mathbb{E}_n[\mathcal{A}] = \mathbb{E}^{T_b}[\mathcal{A}] + \sum_{k \geq 2} \alpha_k^{(t=0)} \beta_k^{\mathcal{A}} \Lambda_k^n, \tag{21}$$

$$\beta_k^{\mathcal{A}} = \langle O_k^b | \mathcal{A} \rangle, \tag{22}$$

$$\alpha_k^{(t=0)} = \sum_{\boldsymbol{x} \in \Omega} P_{\boldsymbol{x}}^{(n=0)} \mathcal{O}_k^b(\boldsymbol{x}). \tag{23}$$

B. The lazy discrete-time dynamics

Let us now assume that we modify our discrete-time dynamics in the following way. At each time step, with probability ϵ we attempt to modify the system exactly as explained in Sec. I A, while with probability $1 - \epsilon$ we do nothing. The rationale for this modification is the following: We want ϵ to represent a very small time step (remember that our final goal is formulating a continuous time dynamics). Of course, in a very short time interval it is highly unlikely that the system changes.

Mathematically, the matrix T_ϵ that represents the lazy dynamics can be simply written in terms of the identity matrix $\mathbb{I}$ and the matrix T considered in Sec. I A

$$T_\epsilon = (1 - \epsilon) \mathbb{I} + \epsilon T, \tag{24}$$

or, better,

$$T_\epsilon = \mathbb{I} + \epsilon \widetilde{R}, \quad \widetilde{R} = T - \mathbb{I}. \tag{25}$$

Mind that the off-diagonal elements of T and $\widetilde{R}$ are identical while, in terms of $\widetilde{R}$, the completeness relation (8) reads

$$\widetilde{R}_{\boldsymbol{x},\boldsymbol{x}} = - \sum_{\boldsymbol{y} \in \Omega \backslash \{\boldsymbol{x}\}} \widetilde{R}_{\boldsymbol{x},\boldsymbol{y}}, \quad \forall \boldsymbol{x} \in \Omega. \tag{26}$$

It is also crucial that $\widetilde{R}$ and T share the orthogonal basis of right eigenvectors $(\mathbf{1}, \mathcal{O}_2^b, \mathcal{O}_3^b, \ldots)$, as well as the basis of left eigenvectors $(\boldsymbol{\pi}^{T_b}, \boldsymbol{v}_2, \boldsymbol{v}_3, \ldots)$.

Thus, Eqs. (20)–(23) carry over to the case of the lazy dynamics with the only change that the eigenvalues Λ_k of the matrix T need to be replaced by the eigenvalues $\Lambda_{k,\epsilon}$ of the matrix T_ϵ. Both sets of eigenvalues can be expressed in terms of the eigenvalues $\widetilde{\lambda}_k$ of the matrix $\widetilde{R}$ (remember that these three matrices, T, T_ϵ and $\widetilde{R}$ share both bases of left and right eigenvectors):

$$\widetilde{\lambda}_k = \Lambda_k - 1, \tag{27}$$

$$\Lambda_{k,\epsilon} = 1 + \epsilon \widetilde{\lambda}_k, \tag{28}$$

where

$$0 = \widetilde{\lambda}_1 \geq \widetilde{\lambda}_2 \geq \ldots \geq \widetilde{\lambda}_{|\Omega|} \geq -2. \tag{29}$$

Hence, for $\epsilon < 1/2$, all the eigenvalues of T_ϵ are guaranteed to be positive.

C. The continuous-time dynamics

We shall reach the limit of continuous time by making the parameter ϵ in Eq. (24) arbitrarily small. Let us start by considering that we need to reach a time t such that t/τ_0 is a rational number (τ_0 is our time unit)

$$\frac{t}{\tau_0} = \frac{p}{q} \in \mathbb{Q}, \tag{30}$$

where p/q is an irreducible fraction (the case of irrational values of t/τ_0 will be trivially solved by continuity through our final formulae). Next, we set a sequence of ϵ_r going to zero as

$$\epsilon_r = \frac{1}{qr}, \quad r \in \mathbb{N}. \tag{31}$$

So, fixing the number of time steps n_r as

$$n_r = Npr, \tag{32}$$

we find that $n_r \epsilon_r = Nt/\tau_0$, irrespective of r. The rationale for introducing the factor of N is that we are already planning to work with a single spin-flip dynamics, hence we wish to work with an extensive number of spin-flip attempts [cf. Eq. (14)].

Eqs. (20) and (21) now take the form [the numerical coefficients $\beta_k^{\mathcal{A}}$ and $\alpha_k^{(t=0)}$ are the same of Eq. (22)/(23), respectively]

$$\boldsymbol{P}^{(n_r)} = \boldsymbol{\pi}^{T_b} + \sum_{k \geq 2} (1 + \epsilon_r \widetilde{\lambda}_k)^{n_r} \gamma_k \boldsymbol{v}_k, \tag{33}$$

$$\mathbb{E}_{n_r}[\mathcal{A}] = \mathbb{E}^{T_b}[\mathcal{A}] + \sum_{k \geq 2} \alpha_k^{(t=0)} \beta_k^{\mathcal{A}} (1 + \epsilon_r \widetilde{\lambda}_r)^{n_r}. \tag{34}$$

Now, the limit of continuous time is reached by letting r go to infinity, so that ϵ_r goes to zero:

$$\lim_{r \to \infty} (1 + \epsilon_r \widetilde{\lambda}_r)^{n_r} = e^{N \widetilde{\lambda}_k t / \tau_0} . \qquad (35)$$

(Recall that the eigenvalues $\widetilde{\lambda}_k$ are nonpositive.) Our final expressions follow:

$$\boldsymbol{P}^{(n_r)} = \boldsymbol{\pi}^{T_b} + \sum_{k \geq 2} e^{-N|\widetilde{\lambda}_k|t/\tau_0} \gamma_k \boldsymbol{v}_k , \qquad (36)$$

$$\mathbb{E}_{n_r}[\mathcal{A}] = \mathbb{E}^{T_b}[\mathcal{A}] + \sum_{k \geq 2} \alpha_k^{(t=0)} \beta_k^{\mathcal{A}} e^{-N|\widetilde{\lambda}_k|t/\tau_0} . \qquad (37)$$

In order to make contact with the expressions in the main text, we just need to redefine our matrix $\widetilde{R}$ and the corresponding eigenvalues as

$$R^{\mathrm{HB}} = N \widetilde{R} , \qquad (38)$$

$$\lambda_k = N \widetilde{\lambda}_k . \qquad (39)$$

D. Practical recipes and description of our computations

Given that in our Ising spin chain $|\Omega| = 2^N$, we can carry out a fully analytical computation only for moderate values of N, say $N \leq 12$. For larger values of N, we have turned to a MC method. Let us explain the two approaches separately. For simplicity, we will denote hereafter the matrix R^{HB} as R.

1. Exact diagonalization

It is crucial to observe from Eqs. (25) and (38) that the matrix R does not depend on ϵ in any way. Hence, we can obtain R directly in the limit of a continuous-time dynamics.

For an Ising chain of length N, R is a $2^N \times 2^N$ square matrix. Indeed, it is a very sparse matrix because only $N + 1$ elements in each row are non vanishing. The N nonvanishing off-diagonal elements are those where the initial configuration $\boldsymbol{x}$ and the final one $\boldsymbol{y}$ differ by a single spin-flip. These nonvanishing off-diagonal matrix elements are identical to the probabilities for accepting the corresponding spin-flip in Eq. (12). The diagonal elements are given, instead, by the completeness relation:

$$R_{\boldsymbol{x}, \boldsymbol{x}} = - \sum_{\boldsymbol{y} \in \Omega \setminus \{\boldsymbol{x}\}} R_{\boldsymbol{x}, \boldsymbol{y}} , \quad \forall \boldsymbol{x} \in \Omega. \qquad (40)$$

We compute the eigenvalues and right eigenvectors of the matrix R using MATHEMATICA. In the first step, we calculated the matrix R and the probability density $\boldsymbol{\pi}^{T_b}$ symbolically as functions of the couplings (J, h), and the bath temperature T_b. We then checked symbolically their basic properties: detailed balance, $R \boldsymbol{1} = \boldsymbol{0}$, and

$\boldsymbol{\pi}^{T_b} R = \boldsymbol{0}$, where $\boldsymbol{0}$ is the constant zero function; i.e., $\boldsymbol{0}(\boldsymbol{x}) = 0$ for all $\boldsymbol{x} \in \Omega$.

The second step consists in evaluating the symbolic expressions for R and $\boldsymbol{\pi}^{T_b}$ with high precision (i.e., 300-digit arithmetic). We then compute the eigenvalues $(0, \lambda_2, \lambda_3, \ldots)$ and right eigenvectors $(\boldsymbol{1}, \mathcal{O}_2^b, \mathcal{O}_3^b, \ldots)$ of R. This is achieved by following Ref. [2, proof of Lemma 12.2]: if D is the diagonal matrix whose diagonal elements are $D_{\boldsymbol{x}, \boldsymbol{x}} = (\pi_{\boldsymbol{x}}^{T_b})^{1/2}$, then the matrix R is similar to the symmetric (and real) matrix $A = D R D^{-1}$. The spectral theorem for this kind of matrices ensures the existence of an *orthonormal* basis of right eigenvectors $\{\mathcal{P}_k\}_{k=1}^{|\Omega|}$ with respect to the inner product

$$\langle \mathcal{A} \mid \mathcal{B} \rangle_0 = \sum_{\boldsymbol{x} \in \Omega} \mathcal{A}(\boldsymbol{x}) \mathcal{B}(\boldsymbol{x}) , \qquad (41)$$

and such that the eigenvector $\mathcal{P}_k$ corresponds to the eigenvalue λ_k. This is so, because if we define $\mathcal{O}_k^b = D^{-1} \mathcal{P}_k$, then $\mathcal{O}_k^b$ is a right eigenvector of R with eigenvalue λ_k. In this way we obtained the sets $\{\mathcal{O}_k^b\}_{k=1}^{|\Omega|}$ and $\{\lambda_k\}_{k=1}^{|\Omega|}$. Indeed, we verified to high accuracy (e.g., at least 270 digits) that these eigenfunctions form an orthonormal basis with respect to the inner product (1), and they satisfied that $R \mathcal{O}_k^b = \lambda_k \mathcal{O}_k^b$ for all k.

The final step needs the initial temperature T_0 of the process. For this temperature, we compute the initial probability density $\boldsymbol{P}^{(t=0)}$ as the Boltzmann weight at temperature T_0. Then we can compute the numerical constants $\alpha_k^{(t=0)}$ (23). Moreover, for all the observables $\mathcal{A}$ we want to consider, we also compute the constants $\beta_k^{\mathcal{A}}$ (22). Now we can obtain the evolution of the expected value of $\mathcal{A}$ with time [cf. (37)]

$$\mathbb{E}_t[\mathcal{A}] = \mathbb{E}^{T_b}[\mathcal{A}] + \sum_{k \geq 2} \alpha_k^{(t=0)} \beta_k^{\mathcal{A}} e^{-|\lambda_k|t} , \qquad (42)$$

where we have chosen units such that $k_B = \tau_0 = 1$. With this choice, the time is in units of a lattice sweep. Using this procedure, we have been able to deal with systems of length $N \leq 12$; notice that for $N = 12$, $\dim(R) = 4\,096$. For the next system length $N = 14$, $\dim(R) = 16\,384$, which is beyond our computing capabilities.

2. The Monte Carlo Algorithm

In order to obtain a workable MC method one just needs to go back to Sec. I C, and compute the probability of not making any change whatsoever to configuration $\boldsymbol{x}$ in a time interval t. It is straightforward to show that

$$\lim_{r \to \infty} [T_{\epsilon_r}^{n_r}]_{\boldsymbol{x}, \boldsymbol{x}} = e^{-|R_{\boldsymbol{x}, \boldsymbol{x}}|t/\tau_0} . \qquad (43)$$

Hence, the probability for the time of the first change to the configuration is the one of a Poisson process, and we are in the canonical situation for an n-fold way simulation [4, 5]. For the reader convenience, let us briefly recall how one such simulation is carried-out.

Let us imagine that we want to update our system for times $t \in [t_1, t_2]$ starting from the configuration $\boldsymbol{x}_{\mathrm{ini}}$ at time t_1. So, we first set our clock to $t = t_1$, and carry out the following procedure (we name $\boldsymbol{x}$ the current spin configuration):

1. Select a time increment

$$\Delta t \;=\; \frac{\tau_0}{|R_{\boldsymbol{x},\boldsymbol{x}}|} \, \log(u) \qquad (44)$$

where u is a uniformly distributed random number in the unit interval $(0, 1]$.

2. If $t + \Delta t > t_2$, stop the simulation [if some observable is to be computed for a time $t' \in (t, t_2)$, it can be computed on the final spin configuration]. If $t + \Delta t < t_2$, go to (3).

3. Update the clock of the simulation $t \to t + \Delta t$. Note that the spin configuration is constant for all times $t' \in (t, t + \Delta t)$. So, if we are to compute an observable for such a t', it should be computed *before* the spin configuration changes.

4. Choose the spin to be flipped with probability $R_{\boldsymbol{x},\boldsymbol{y}}/|R_{\boldsymbol{x},\boldsymbol{x}}|$ (mind that if $t + \Delta t > t_2$ this step should be skipped). Remember that $R_{\boldsymbol{x},\boldsymbol{y}} \neq 0$ only if the new state $\boldsymbol{y}$ differs from the old state $\boldsymbol{x}$ precisely by one spin-flip. Set the chosen state $\boldsymbol{y}$ as the new current state.

5. Return to (1).

For an Ising chain, there is a simple technical trick to considerably speed up the simulation. Indeed, Eq. (12) tells us that the $R_{\boldsymbol{x},\boldsymbol{y}}$ depends only on the energy change when flipping one of the spins in the starting configuration $\boldsymbol{x}$. Now, the energy-change upon flipping the spin σ_k depends solely on $\sigma_{k-1} + \sigma_{k+1}$ (three possible values: $2, 0, -2$), and on the value of $\sigma_k = \pm 1$. Hence, according to the energy change caused by their spin flip, there are only 3×2 possible kind of spins. Therefore, in order to compute Δt and to decide efficiently which spin to update, it suffices to maintain an updated set of six list of spins (one for every kind of spins).

3. Our simulations

We generate a large number of statistically independent trajectories S. On each trajectory we consider observables $\mathcal{A}$ [see, for instance, Eqs. (4) and (5)]. We also select a priori a mesh of measuring times $\{t^{(1)}, \ldots, t^{(M)}\}$. For each of this times, $t^{(k)}$ and for each trajectory s, we obtain the corresponding value

$$\mathcal{A}_{k,s} \;\equiv\; \mathcal{A}[\boldsymbol{x}^{(s)}(t^{(k)})] \qquad (45)$$

where $\boldsymbol{x}^{(s)}(t^{(k)})$ is the configuration of the s-th trajectory at time $t^{(k)}$. The expected value $\mathbb{E}_{t^{(k)}}[\mathcal{A}]$ is estimated as

$$\mathbb{E}_{t^{(k)}}[\mathcal{A}] \;=\; \frac{1}{S} \sum_{s=1}^{S} \mathcal{A}_{k,s} \,, \qquad (46)$$

Simulation $T_b, (T_q)$	Size	Trajectories	Replicas	Time
$15.177 \to 1$	8,12,32	2×10^7	120	10
$4.15 \to 1$	8,12,32	2×10^7	120	10
$1 \to 15.177$	8,12,32	2×10^7	120	10
$4.15 \to 15.177$	8,12,32	2×10^7	120	10
$15.177 \to 4.15$	8,12,32	2×10^7	120	8
$1 \to 4.15$	8,12,32	2×10^7	120	8
$4.15 \to (2000) \to 1$	8,12,32	2×10^7	120	10 (0.156)

TABLE I. List of simulations. Columns: (I) Bath temperatures used in each case simulated. Parentheses indicate the temperature used during the first step in the preheating protocol. (II) Number of spins in the chain. (III) Number of independent trajectories simulated per replica. (IV) Independent simulated copies of the system. (V) Time length in units such that $\tau_0 = 1$. Parentheses indicate the time in contact with the first thermal bath during the preheating protocol.

while we compute errors for these expected values in the standard way:

$$\Delta \mathbb{E}_{t^{(k)}}[\mathcal{A}] \;=\; \sqrt{\frac{1}{S(S-1)} \sum_{s=1}^{S} \left(\mathcal{A}_{k,s} - \mathbb{E}_{t^{(k)}}[\mathcal{A}] \right)^2} \,. \quad (47)$$

All our trajectories contain a preparation step and a measuring step. In the preparation step, the initial configurations for the trajectories are chosen randomly with uniform probability. Hence, the dynamics sketched in the previous paragraph is followed at the initial temperature for a time long enough to ensure equilibration. Then, one (or more) temperature jumps are carried out. This amounts to changing the acceptance in Eq. (12), while taking as the initial configuration at the new temperature, the final configuration at the previous temperature.

Technical simulation details are shown in Table I. The simulations were performed in PROTEUS cluster, the supercomputing center of the Institute Carlos I for Theoretical and Computational Physics at University of Granada. In particular, for each replica nodes of 12 processors at 3.45GHz and 16Mb of memory were used. The parameters of the simulations were $J = -4$, $h = 8.2$, and we choose time units such that $\tau_0 = 1$. The values presented in the main manuscript were obtained averaging a total number of 2.4×10^9 trajectories.

II. EXACT EXPECTATION VALUES FOR SOME QUANTITIES

In order to present these expectation values, we first need to introduce some notation. Let us define the couplings

$$K \;=\; \frac{J}{k_B T}, \qquad H \;=\; \frac{h}{k_B T}. \qquad (48)$$

All the following mean values depend on both quantities and on the spin chain length N (recall that in our units, $k_B = 1$).

Basically, we will use the transfer-matrix method in this computation. We first define the coefficient $\psi = \psi(K, H)$ as the ratio of the two eigenvalues of the transfer matrix:

$$\psi(K, H) = \frac{\cosh(H) - \sqrt{e^{-4K} + \sinh^2(H)}}{\cosh(H) + \sqrt{e^{-4K} + \sinh^2(H)}}. \quad (49)$$

Notice that $|\psi(K, H)| < 1$, so $\lim_{N \to \infty} \psi^N = 0$.

The uniform magnetization is given by

$$M_u = \frac{\sinh(H)}{\sqrt{e^{-4K} + \sinh^2(H)}} \frac{1 - \psi^N}{1 + \psi^N}. \quad (50)$$

The spin-spin interaction is given by

$$C_1 = \frac{\sinh^2(H)}{e^{-4K} + \sinh^2(H)}$$

$$+ \frac{1 + \psi^{N-2}}{1 + \psi^N} \frac{\psi}{1 + e^{4K} \sinh^2(H)}. \quad (51)$$

The internal energy is given by a linear combination of the previous two values

$$E = -J C_1 - h M_u. \quad (52)$$

The staggered susceptibility is given for a spin chain of even length by

$$\chi_{\text{st}} = \frac{e^{-4K}}{\cosh(H) \sqrt{e^{-4K} + \sinh^2(H)}} \frac{1 - 2\psi^N}{1 + \psi^N}. \quad (53)$$

III. SOME ADDITIONAL RESULTS FOR THE 1D ISING MODEL

In this section we will describe some results related to the three anomalous phenomena discussed in the main text.

A. The Markovian Mpemba effect

Figure 1 illustrates the ME as obtained with $T_b = 1$, $T_c = 4.15$, and $T_h = 15.177$. Let us define for simplicity the quantity $\Delta_t[\mathcal{A}] = (\mathbb{E}_t^h[\mathcal{A}] - \mathbb{E}_t^c[\mathcal{A}])/N$ for any observable. We will consider the two observables not discussed in the main text; namely, $\mathcal{A} \in \{\mathcal{M}_{\text{st}}^2, \mathcal{M}_u\}$.

In Fig. 1(a) we see that there is no crossing for $\mathcal{M}_{\text{st}}^2$; this is expected as we have prepared our system so that $\mathbb{E}_t^h[\mathcal{M}_{\text{st}}^2]$ is exponentially accelerated with respect to $\mathbb{E}_t^c[\mathcal{M}_{\text{st}}^2]$. Hence, the negative sign in Fig. 1(a). On the other hand, in Fig. 1(b), we see a crossing similar to those displayed in Fig. 3 of the main text: there is ME for the observable $\mathcal{M}_u$.
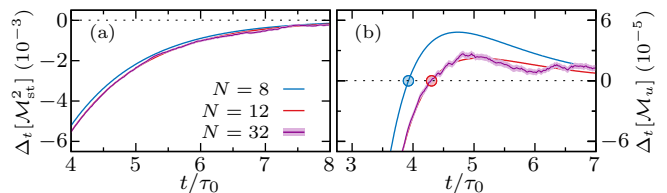

FIG. 1. Mpemba effect. Evolution of $\Delta_t[\mathcal{A}]$ for the observables $\mathcal{A} = \mathcal{M}_{\text{st}}^2$ (a), and $\mathcal{A} = \mathcal{M}_u$ (b). We show the results for $N = 8$ (blue), $N = 12$ (red), and $N = 32$ (purple, with a lighter shade representing the error bars of the MC data). In panel (b), the time at which $\Delta_t[\mathcal{M}_u]$ changes sign is marked by a dot.

B. Preheating for faster cooling

In this section, we compare the one-step protocol against a two-step protocol. In the former, we start with system in equilibrium at temperature $T_0 = 4.15$, and we let this system evolve with a bath temperature $T_b = 1$. In the latter, we start again at T_0, but we first let the system to evolve with a bath at temperature $T_q = 2000$ up to $t = t_w = 0.156$; at this time, we put the system instantaneously in contact with a another bath at temperature $T_b = 1$. We expect that this second preheating protocol will make the system to evolve faster than the standard one-step protocol. It is now useful to define $\delta_t[\mathcal{A}] = |\mathbb{E}_t[\mathcal{A}] - \mathbb{E}^{T_b}[\mathcal{A}]|/N$.

Figure 2 shows that preheating speeds up the evolution of the two observables not reported in the main text, namely, $\mathcal{A} \in \{\mathcal{E}, \mathcal{M}_u\}$. For the energy, this behavior is clear for the exact data ($N = 8, 12$), but for $N = 32$ the results after $t \approx 6.5$ are less definitive due to the large error bars of the MC results.
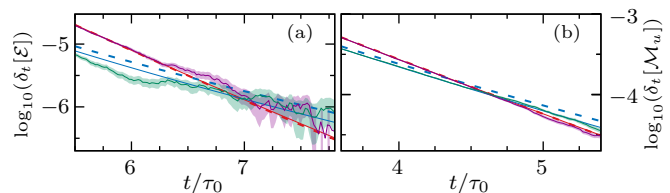

FIG. 2. Preheating strategy for faster cooling. Evolution of $\delta_t[\mathcal{A}]$ for $\mathcal{A} = \mathcal{E}$ (a), and $\mathcal{A} = \mathcal{M}_u$ (b). Colors red and purple (respectively blue and green) denote that the protocol includes (respectively does not include) an initial quench at temperature T_q. We show data for $N = 8$ (dashed lines), $N = 12$ (solid lines), and $N = 32$ (solid lines with a lighter shade representing the error bars of the MC data). Both panels show the expected speedup for the preheating protocol, although in (a) the error bars for $N = 32$ are rather large to draw a definitive conclusion.
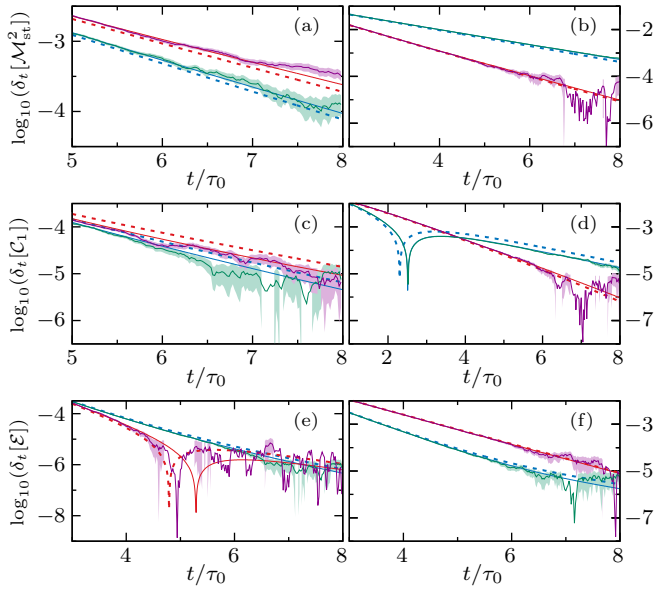
FIG. 3. (A)symmetry in heating and cooling. Evolution of $\delta_t[\mathcal{A}]$ for $\mathcal{A} = \mathcal{M}_{\text{st}}^2$ (a,b), $\mathcal{A} = \mathcal{C}_1$ (c,d), and $\mathcal{A} = \mathcal{E}$ (e,f). In each panel, we depict cooling (blue and green) and heating (red and purple) processes. We show data for $N = 8$ (dashed lines), $N = 12$ (solid lines), and $N = 32$ (solid lines with a lighter shade representing the errors of the MC data). The cooling and heating processes were carried out between: (a,c,e) $T_A = 1$ and $T_B = 4.15$; and (b,d,f) $T_A = 15.177$ and $T_B = 4.15$. For $\mathcal{M}_{\text{st}}^2$ and $\mathcal{C}_1$, it is slower to approach $T_B = 4.15$: i.e., to heat up in (a,c), and to cool down in (b,d). However, the behavior is the opposite for the energy (e,f).

C. Heating and cooling may be asymmetric processes

Here we will compare the behavior of starting at $T = T_A$ and evolving to the bath temperature $T = T_B$ against the inverse process: i.e., starting at $T = T_B$ and evolving to the bath temperature $T = T_A$. We have made two experiments: one with $T_A = 1$ and $T_B = 4.15 \approx T_b^*$ (see left panels in Fig. 3), and the other one with $T_A = 15.177$ and $T_B = 4.15$ (see right panels in Fig. 3). Here T_b^* is the temperature at which the staggered susceptibility χ_{st} attains a maximum [see Fig. 2(a) of the main text].

In Fig. 3 we show the data not reported in the main text, and corresponding to the observables $\mathcal{A} \in \{\mathcal{M}_{\text{st}}^2, \mathcal{C}_1, \mathcal{E}\}$ in panels (a,b), (c,d), and (e,f), respectively. Note that in panel (d), we observe a change of sign at $t \approx 2.5$ in the quantity $\mathbb{E}_t[\mathcal{C}_1] - \mathbb{E}^{T_b = T_B}[\mathcal{C}_1]$ for the system originally at $T_A = 15.177$. We also observe such a change of sign in panel (e) for the quantity $\mathbb{E}_t[\mathcal{E}] - \mathbb{E}^{T_b = T_B}[\mathcal{E}]$ at $t \approx 5$ for the system originally at $T_A = 1$.

We observe in Fig. 3(a,b,c,d), as we did in the main text for the observable $\mathcal{M}_u$, that for observables $\mathcal{M}_{\text{st}}^2$ and $\mathcal{C}_1$, it is always *faster* to move away from $T_B = 4.15$ and approach T_A: i.e., to cool down in (a,c), and to heat up in (b,d).

However the behavior for the energy $\mathcal{E}$ is the opposite [see Fig. 3(e,f)]: it is faster to approach $T_B = 4.15$: i.e., to heat up in (e) and to cool down in (f). The explanation of this effect was already given in the main text: for bath temperatures close to $T_B = 4.15 \approx T_b^*$, the coefficient $\beta_2^{\mathcal{E}} \approx 0$ [cf. Eq. (22)].

[1] A. D. Sokal, *In Functional Integration: Basics and Applications (1996 Cargèse School)*, edited by C. DeWitt-Morette, P. Cartier, and A. Folacci (Plenum, New York, 1997).

[2] D. A. Levin and Y. Peres, *Markov Chains and Mixing Times*, Vol. 107 (American Mathematical Soc., Providence, 2017).

[3] Our definition of lazy dynamics is a generalization of the definition introduced in Sec. 1.3 of Ref. [2].

[4] A. B. Bortz, M. H. Kalos, and J. L. Lebowitz, J. Comp. Phys. **17**, 10 (1975).

[5] D. T. Gillespie, J. Phys. Chem. **81**, 2340 (1977).

[6] For complex observables, one would modify Eq. (1) as $\langle \mathcal{A} | \mathcal{B} \rangle = \sum_{\boldsymbol{x} \in \Omega} \pi_{\boldsymbol{x}}^{T_b} \overline{\mathcal{A}(\boldsymbol{x})} \mathcal{B}(\boldsymbol{x})$, where the over-line stands for complex conjugation.

[7] The reverse statement is not true: stationary does not entail detailed balance.

[8] For any square matrix, it is possible to find a basis of the vector space formed solely by left eigenvectors if, and only if, it is also possible to find a basis of right eigenvectors. Furthermore, the spectrum of left eigenvalues is identical to the spectrum of right eigenvalues.

[9] Therefore, the approach to equilibrium means that $\mathcal{T}^n[\mathcal{A}]$ approaches $\mathbb{E}^{T_b}[\mathcal{A}]\mathbf{1}$ as n grows. In other words, after many time steps, the expected value for $\mathcal{A}$ becomes the equilibrium expectation value at temperature T_b, irrespective of the starting configuration $\boldsymbol{x}$.